

Limits on the ions temperature anisotropy in turbulent intracluster medium

R. Santos-Lima,^{1,2,3*} H. Yan,^{1,2†} E. M. de Gouveia Dal Pino,³ and A. Lazarian⁴

¹DESY, Platanenallee 6, 15738 Zeuthen, Germany

²Institut für Physik und Astronomie, Universität Potsdam, 14476 Potsdam-Golm, Germany

³Instituto de Astronomia, Geofísica e Ciências Atmosféricas, Universidade de São Paulo, R. do Matão, 1226, São Paulo, SP 05508-090, Brazil

⁴Department of Astronomy, University of Wisconsin, 475 North Charter Street, Madison, WI 53706, USA

Last updated 2015 May 22; in original form 2013 September 5

ABSTRACT

Turbulence in the weakly collisional intracluster medium of galaxies (ICM) is able to generate strong thermal velocity anisotropies in the ions (with respect to the local magnetic field direction), if the magnetic moment of the particles is conserved in the absence of Coulomb collisions. In this scenario, the anisotropic pressure magnetohydrodynamic (AMHD) turbulence shows a very different statistical behaviour from the standard MHD one and is unable to amplify seed magnetic fields, in disagreement with previous cosmological MHD simulations which are successful to explain the observed magnetic fields in the ICM. On the other hand, temperature anisotropies can also drive plasma instabilities which can relax the anisotropy. This work aims to compare the relaxation rate with the growth rate of the anisotropies driven by the turbulence. We employ quasilinear theory to estimate the ions scattering rate due to the parallel firehose, mirror, and ion-cyclotron instabilities, for a set of plasma parameters resulting from AMHD simulations of the turbulent ICM. We show that the ICM turbulence can sustain only anisotropy levels very close to the instabilities thresholds. We argue that the AMHD model which bounds the anisotropies at the marginal stability levels can describe the Alfvénic turbulence cascade in the ICM.

Key words: galaxies: clusters: intracluster medium – (*magnetohydrodynamics*) MHD – turbulence – plasmas

1 INTRODUCTION

The intracluster medium of galaxies (ICM) is composed by a plasma weakly collisional and magnetized, with turbulent motions at the large scales. The cosmological mergers of sub-clusters are thought to be the major sources of turbulence in the ICM. The turbulence time-scale for the ICM is $\tau_{turb} \sim 10^{16}$ sec (using $L_{turb} = 500$ kpc and $U_{turb} = 10^3$ km/s as the length scale and velocity of the largest scale turbulent motions) while the time-scale for the Coulomb collisions between ions is estimated as $\tau_i \sim 10^{15}$ sec¹ (mean-free-path of ~ 30 kpc for the ion-ion collisions), which requires a nearly collisionless approach.

The conservation of the first adiabatic invariant of the charged particles (magnetic moment) combined with the large scale plasma motions stretching/compressing the magnetic fields in the ICM leads to the development of

differences between the parallel (to the local field lines) and the gyro component of the thermal velocities of the ions. Therefore, being highly turbulent and weakly collisional, the ICM naturally develops anisotropies in the local distribution of the ions thermal velocities. This anisotropy is a source of free energy, which can trigger electromagnetic plasma instabilities (such as ion-cyclotron, mirror, and firehose; see for example Gary 1993) playing a very important role on the dynamics of the system and on the turbulence evolution itself (Schekochihin & Cowley 2006; Kowal, Falceta-Gonçalves, & Lazarian 2011; Santos-Lima et al. 2014; Mogavero & Schekochihin 2014). Nonetheless, such a role remains still poorly understood.

An anisotropic magnetohydrodynamic (AMHD) approximation that assumes a bi-Maxwellian distribution of thermal velocities, i.e., takes into account two independent temperature components (one for the thermal velocity parallel to the local magnetic field and another for the gyro-motion of the particles), can be employed in this situation. The solutions of the AMHD equations reveals some linear instabilities (mirror and firehose), cor-

* Contact e-mail: reinaldo.santos.de.lima@desy.de

† Contact e-mail: huirong.yan@desy.de

¹ Considering the ions temperature $T_i = 10$ keV, density $n = 10^{-3}$ cm⁻³, and the Coulomb logarithm $\ln \Lambda = 20$.

responding to the large wave-length (fluid) limit of these plasma instabilities (see for example [Hau & Wang 2007](#); [Kowal, Falceta-Gonçalves, & Lazarian 2011](#)).

The effects of anisotropy driven instabilities at the micro-scales are still a matter of debate. In one scenario, the plasma instabilities saturate the anisotropy at low levels, close to the instabilities thresholds (see e.g. [Mogavero & Schekochihin 2014](#)). In another scenario, if the anisotropy survives during the dynamical time-scales and anisotropic thermal stresses dominate the dynamics of the system, there is a change in the traditional MHD turbulence picture with the presence of instabilities at fluid scales. Studies of the turbulence statistics and the magnetic field amplification applying the last scenario to galaxy clusters ([Kowal, Falceta-Gonçalves, & Lazarian 2011](#); [Santos-Lima et al. 2014](#); [Falceta-Gonçalves & Kowal 2015](#)) as well as to the Earth's magnetosphere ([Meng et al. 2012](#)) revealed drastic differences compared to the isotropic MHD approach. Nevertheless in this case the numerical description is incomplete, as the instabilities that should develop at the subgrid scales may influence the large scale anisotropy evolution (see [Mogavero & Schekochihin 2014](#) and discussion in Section 6.4).

All these collisionless effects possibly influence the Cosmic-Ray (CR) propagation and acceleration in the ICM. For instance, compressible modes rather than Alfvénic turbulence have been identified as the dominant agent for particle acceleration ([Yan & Lazarian 2002](#)). In the absence of the anomalous scattering of the ions produced by the kinetic instabilities, the large parallel viscosity of the ions will damp efficiently the compressible modes in the ICM. At the same time, if magnetic fluctuations caused by the temperature anisotropy are present in the large scale ICM, they could have direct impact on the propagation of Cosmic-Rays in the medium (e.g. [Nakwacki & Peralta-Ramos 2013](#)).

Obviously, the effects of the plasma instabilities at the kinetic scales cannot be captured by any MHD model (see discussion in Section 6.4 about the general effects of the subgrid phenomena). The impact of a fast thermal relaxation due to particle scattering by the kinetic instabilities on the turbulence cascade and on the magnetic field amplification was also investigated in [Santos-Lima et al. \(2014\)](#), where the rate of this process was considered as a free-parameter. The pitch-angle scattering rate caused by some of these instabilities has been investigated for the solar wind via two-dimensional PIC and hybrid (PIC-MHD) simulations ([Gary, Yin, & Winske 2000](#)) and also via a quasilinear approach ([Seough & Yoon 2012](#); [Yoon & Seough 2012](#)), and the results point to a scattering time of the order of the linear growth rate of the instabilities (which can be \sim ion kinetic times-scales). In fact, these studies only considered the evolution of the instabilities starting from an unstable anisotropy level (see Section 6.2). In the situation of a very slow driving of the thermal anisotropy (compared to the ion thermal gyrofrequency), recent two-dimensional PIC simulations ([Riquelme et al. 2012](#); [Riquelme, Quataert, & Verscharen 2015](#)) and hybrid ([Kunz, Schekochihin, & Stone 2014](#); [Melville, Schekochihin, & Kunz 2016](#)) have demonstrated that the anisotropy relaxation arising from the instabilities do not necessarily result in instantaneous anomalous scat-

tering of the ions during the time of anisotropy driving by the turbulent motions (see Section 6.3).

Nonetheless, a self-consistent treatment of the feedback of these instabilities connected to the turbulence cascade is still missing. A guiding procedure was developed relating consistently both plasma instabilities induced by high energy CR (gyroresonance instability) and the turbulence in the interstellar and intergalactic media ([Lazarian & Beresnyak 2006](#); [Yan & Lazarian 2011](#)).

The aim of this work is to evaluate the limits on the temperature anisotropy particularly in the turbulent intergalactic or intra-cluster medium taking into account the scattering produced by the electromagnetic instabilities triggered by temperature anisotropy in an approach similar to the work by [Yan & Lazarian \(2011\)](#). For this goal, we will compare directly the ions scattering rate obtained from quasilinear theory with the anisotropy generation rate by turbulence obtained from AMHD simulations ([Santos-Lima et al. 2014](#)).

This study is organized as follows: in §2 we review the observed relation between the bounds on the temperature anisotropy in the solar wind and the collisionless instabilities; in §3 we describe briefly the AMHD simulations used in this work, and in §4 we present the quasilinear equations employed for calculating the scattering rate of the ions; in §5 we present the results. In §6 we discuss some limitations and consequences of our study and we relate it to other works; and finally in §7 we summarize and conclude our analysis.

2 EMPIRICAL BOUNDS ON THE TEMPERATURE ANISOTROPY

The distribution function of the thermal velocities of the species in the nearly collisionless plasmas of the Earth's magnetosphere is accessible via direct measurements by spacecrafts. The data accumulated from the last decades have shown that the electrons and ions in the solar wind at a distance ≈ 1 AU present a bi-Maxwellian distribution, with the maximum anisotropy in the temperatures anti-correlated with the local plasma β , which is the ratio between the thermal and magnetic energy densities (see more details in [Marsch 2006](#) and references therein; [Hellinger et al. 2006](#); [Štverák et al. 2008](#)). These limits on the anisotropy degree are below the expected levels when one assumes adiabatic conservation of the magnetic momentum of the particles p_{\perp}/B (where p_{\perp} is here the perpendicular momentum of the particle and B is the intensity of the magnetic field) during the expansion/compression of the solar wind (see for example [Bale et al. 2009](#)).

These limits are interpreted as resulting from the non-linear saturation of the kinetic instabilities driven by the temperature anisotropy ([Gary 1993](#)). The linear dispersion of a plasma with one or more species having a bi-Maxwellian distribution presents a few instabilities resulting from the temperature anisotropy. The observed limits on the temperature anisotropy have been identified with the approximate thresholds for the firehose, mirror, and ion-cyclotron instabilities (see for example [Hellinger et al. 2006](#); [Bale et al. 2009](#); [Maruca, Kasper, & Gary 2012](#)).

The physical process limiting the temperature anisotropy depends on the specific instability and on

the initial anisotropy level (see discussion in Sections 6.2 and 6.3). After the instabilities growth saturation, this process is understood in terms of collisionless dissipation, with particles being scattered by the collective electromagnetic fluctuations caused by the instabilities (Kunz, Schekochihin, & Stone 2014). These wave-particle interactions (quasi-collisions) diffuse the momentum of the particles and so their pitch angle, relaxing the distribution function towards a Maxwellian one. This effect is not only observed in the solar wind, but also in laboratory plasmas (Keiter 1999) and in fully non-linear plasma simulations (Tajima, Mima, & Dawson 1977; Tanaka 1993; Gary et al. 1997, 1998; Gary, Yin, & Winske 2000; Le et al. 2010; Nishimura, Gary, & Li 2002; Riquelme et al. 2012; Kunz, Schekochihin, & Stone 2014; Riquelme, Quataert, & Verscharen 2015; Sironi & Narayan 2015; Sironi 2015).

3 TEMPERATURE ANISOTROPY DEVELOPMENT IN THE TURBULENT ICM: AMHD SIMULATIONS

In Santos-Lima et al. (2014, SL+14 hereafter), a numerical study of the ICM turbulence was carried out by means of anisotropic MHD simulations of forced turbulence in a periodic box. The temperature anisotropy evolution was modeled via the CGL closure (Chew, Goldberger, & Low 1956) modified by the addition of a phenomenological pitch-angle scattering term:

$$\frac{\partial A}{\partial t} = \left(\frac{\partial A}{\partial t} \right)_{CGL} + \left(\frac{\partial A}{\partial t} \right)_{scatt}, \quad (1)$$

$$\left(\frac{\partial A}{\partial t} \right)_{CGL} = -\nabla \cdot (A\mathbf{u}) + 3A\mathbf{b} \cdot [(\mathbf{b} \cdot \nabla)\mathbf{u}], \quad (2)$$

$$\left(\frac{\partial A}{\partial t} \right)_{scatt} = -\nu_S (2A^2 - A - 1), \quad (3)$$

where $A = T_{\perp}/T_{\parallel}$ is the ratio between the temperature components; \mathbf{u} and \mathbf{B} are respectively the velocity and magnetic fields, with $\mathbf{b} = \mathbf{B}/B$; and ν_S is the pitch-angle scattering rate. The ions and electrons were considered to have identical temperature components, for simplicity. Also for simplicity, the cooling employed was considered not to affect the temperature anisotropy.

The effective scattering rate ν_S accounts for the effect of both the Coulomb collisions and the non-linear particle-plasma wave interactions. In SL+14 the Coulomb collisions were neglected and the scattering was attributed only to the action of the mirror and firehose instabilities whenever the anisotropy A overcame the threshold values for these instabilities. Different values were considered for ν_S , from the limit of no scattering ($\nu_S = 0$) till the extreme case in which the scattering time is very short or infinitely small compared to the resolved timescales of the simulation ($\nu_S = \infty$).

Our purpose here is (i) to provide an evaluation of the scattering rate ν_S due to the plasma instabilities, and (ii) to estimate the limits on the ions anisotropy A_i in the ICM plasma by imposing the statistical equilibrium between the

terms $(\partial A_i/\partial t)_{CGL}$ and $(\partial A_i/\partial t)_{scatt}$. For this aim we will follow three steps: (1) obtain from the MHD turbulence simulation the characteristic time for the anisotropy development $\tau_A = A_i \langle \partial A_i/\partial t \rangle_{CGL}^{-1}$ as a function of the ion plasma parameters A_i and $\beta_{i\parallel}$; (2) estimate $\nu_S(A_i, \beta_{i\parallel})$ using quasilinear theory and then calculate the characteristic time for the anisotropy relaxation $\tau_{\nu} = A_i \langle \partial A_i/\partial t \rangle_{scatt}^{-1}$; (3) find the values of $A_i(\beta_{i\parallel})$ for which $\tau_A = \tau_{\nu}$, in order to estimate the maximum anisotropy level that the turbulence can sustain in the presence of the instabilities scattering².

The AMHD turbulence simulation we employ in step (1) has $\nu_S = 0$ (which is non realistic as it will be seen). It corresponds to the model A1 presented in SL+14. The value of ν_S of the MHD simulation is of little importance in this stage because it should not influence the evaluation of τ_A (at least in order of magnitude), though it changes considerably the spreading of the PDF of the plasma parameters (A, β_{\parallel}) . To confirm this, we also repeated our analysis using an AMHD model with a physically more plausible value of ν_S ($\nu_S \sim 10\tau_{turb}^{-1}$; see below). We consider an uniform magnetic field in the domain; the ratio between the unperturbed thermal pressure and the magnetic pressure of this uniform magnetic field has the value of $\beta_0 = 200$, which is representative of the ICM. Super-Alfvénic and subsonic turbulence (with Alfvénic Mach number $M_A \equiv \langle |\mathbf{u}|/v_A \rangle \approx 1.2$ and sonic Mach number $M_S \equiv \langle |\mathbf{u}|/c_S \rangle \approx 0.6$) is considered with an injection scale $l_{turb} = 0.4L_0$, where L_0 is the computational box size. The employed resolution (512^3) allows for solving a modest inertial range covering the range of dimensionless wavenumbers $2.5 \lesssim kL_0 \lesssim 20$. Further details on the numerical setup, code, and the turbulence statistics analysis can be found in SL+14.

We define the following physical dimensions for our simulations: $L_0 = 100$ kpc is the box size, $\rho_0 = 10^{-27}$ g/cm³ is the mean density, and $c_{S0} = 10^8$ cm/s is the unperturbed thermal speed (corresponding to the gas temperature $T_0 \approx 6 \times 10^8$ K). With this choice of units, $l_{turb} = 40$ kpc, $u_{rms} \approx 7 \times 10^7$ cm/s, and $B_0 = 3$ μ G is the intensity of the mean magnetic field, corresponding to the ion thermal gyrofrequency $\Omega_{i0} \approx 3 \times 10^{-2}$ s⁻¹.

4 QUASILINEAR EVOLUTION OF THE KINETIC INSTABILITIES

The electromagnetic waves in the plasma can interact with the particles, exchanging energy and momentum. This process can be described statistically as a diffusion of the distribution function in the velocity space.

In a collisionless plasma composed by ions (protons) and electrons, the electromagnetic fluctuations driven by thermal anisotropy more important for the scattering of the ions are generated by the firehose, mirror, and ion-cyclotron instabilities (Gary 1993). The firehose instability can be excited when $T_{i\perp} < T_{i\parallel}$, and the mirror and ion-cyclotron

² Rigorously speaking, the maintenance of the marginal state during the simultaneous anisotropy driving and relaxation should also take into account the evolution of the local magnetic field intensity. For example, the mirror instability is set theoretically for $A > 1 + \beta_{\perp}^{-1}$; therefore, to keep the plasma in the marginal state requires $(\partial A/\partial t)_{CGL} + (\partial A/\partial t)_{scatt} \leq (\partial \beta_{\perp}^{-1}/\partial t)$.

can be excited in the opposite regime $T_{i\perp} > T_{i\parallel}$. The resulting scattering from these instabilities decreases the temperature anisotropies and consequently regulates the growth of the instabilities themselves. The fastest growth modes for these instabilities occur for scales close to the ion Larmor radius, with growth rates which can be of the order of the ion Larmor frequency. The electrons anisotropy is expected to be relaxed on faster time-scales (by the whistler and firehose modes; see Gary 1993; Nishimura, Gary, & Li 2002; Štverák et al. 2008).

The non-linear development of the instabilities can be investigated analytically using the quasilinear theory, which assumes small perturbations of the distribution functions and of the electromagnetic fields (compared to the zeroth order, background values). The quasilinear theory also assumes the superposition of non-interacting plasma waves with random phases, which satisfy the linear dispersion relation of the plasma. The second order effects of these waves on the particles distribution function give rise to a diffusion term in the momentum space, which can be interpreted as resulting from effective collisions. In Section 6.2 we discuss the limitations of the quasilinear approximation to approach the instabilities evolution.

Hellinger et al. (2013) provide the general quasilinear expressions for the evolution of the mean velocity and thermal energy components of a general drifting bi-Maxwellian plasma composed by protons and electrons. Here we will use the simpler expressions derived in Yoon & Seough (2012) and Seough & Yoon (2012) for a bi-Maxwellian distribution function for the ions and an isotropic distribution for the electrons, for the evolution of the temperature components due to the parallel firehose, mirror, and ion-cyclotron instabilities. Below we reproduce these expressions.

4.1 Parallel firehose modes

The linear dispersion relation for the firehose modes (modes with right-hand circular polarization) propagating parallel to the mean magnetic field is given by:

$$0 = \frac{c^2 k^2}{\omega_{pi}^2} - \frac{\omega_k}{\Omega_i} + \left(1 - \frac{T_{i\perp}}{T_{i\parallel}}\right) - \left[\frac{T_{i\perp}}{T_{i\parallel}} \omega_k - \left(1 - \frac{T_{i\perp}}{T_{i\parallel}}\right) \Omega_i\right] \frac{1}{k v_{i\parallel}} Z\left(\frac{\omega_k + \Omega_i}{k v_{i\parallel}}\right) \quad (4)$$

where $\omega_k = \omega(k)$ is the wave complex frequency for the wave-vector $k = k_{\parallel}$, $\omega_{pi} = \sqrt{4\pi n_i e^2 / m_i}$ and $\Omega_i = e B_0 / m_i c$ are respectively the plasma frequency and Larmor frequency for the ions, $v_{i\parallel} = \sqrt{T_{i\parallel} / m_i}$ is the parallel thermal speed of the ions, $Z(\xi)$ is the plasma function; n_i , e , B_0 , and m_i are the ions density, elementary charge, background magnetic field intensity, and ion mass, respectively. The terms of the order $(\omega_k / \omega_{pi})^2$ and ω_k / Ω_e were neglected in the above dispersion relation.

The evolution equations for the ion kinetic energies (second order moments of the distribution function) resulting from the interaction with the parallel firehose modes are given by

$$n_i \frac{dT_{i\perp}}{dt} = 8 \int_0^\infty dk \gamma_k \frac{|\delta B_k|^2}{8\pi} \left[\frac{\Re(\omega_k) \Omega_i}{k^2 v_A^2} - 1 \right], \quad (5)$$

$$\frac{n_i}{2} \frac{dT_{i\parallel}}{dt} = -4 \int_0^\infty dk \gamma_k \frac{|\delta B_k|^2}{8\pi} \left[\frac{2\Re(\omega_k) \Omega_i}{k^2 v_A^2} - 1 \right], \quad (6)$$

where $v_A = B_0 / \sqrt{4\pi n_i m_i}$ is the Alfvén velocity, $\Re(\omega_k)$ and γ_k are the real and imaginary parts of ω_k , respectively, and $|\delta B_k|^2 / 8\pi$ is the spectral energy density of the magnetic fluctuations, which evolves accordingly to the wave kinetic equation

$$\frac{\partial |\delta B_k|^2}{\partial t} = 2\gamma_k |\delta B_k|^2. \quad (7)$$

We refer to Seough & Yoon (2012) for more details on the deduction of the above equations.

4.2 Ion-cyclotron and mirror modes

The linear dispersion relation for the ion-cyclotron modes (with left-hand side polarization) propagating in an arbitrary oblique direction to the mean magnetic field is given by

$$0 = \frac{c^2 k^2}{\omega_{pi}^2} + \frac{\omega_k^{IC}}{\Omega_i} - 2 \frac{I_1(\lambda) \exp(-\lambda)}{\lambda} \times \left[\xi^{IC} Z(\xi^{IC}) - \left(\frac{T_{i\perp}}{T_{i\parallel}} - 1\right) \frac{Z'(\xi^{IC})}{2} \right], \quad (8)$$

where $\omega_k^{IC} = \omega^{IC}(\mathbf{k})$ is the complex wave-frequency for the two-dimensional wave-vector $\mathbf{k} = (k_{\parallel}, k_{\perp})$, $\xi^{IC} = \omega_k^{IC} / k_{\parallel} v_{i\parallel}$, $\zeta^{IC} = (\omega_k^{IC} - \Omega_i) / k_{\parallel} v_{i\parallel}$, $\lambda = k_{\perp}^2 v_{i\perp}^2 / 2\Omega_i^2$, $v_{i\perp} = \sqrt{2T_{i\perp} / m_i}$, $I_j(\lambda)$ is the modified Bessel function of the first kind of order j , and Z' is the derivative of the plasma function Z .

The dispersion relation of the non-propagating mirror modes is in turn given by

$$0 = \frac{c^2 k^2}{\omega_{pi}^2} + 2\lambda [I_0(\lambda) - I_1(\lambda)] \times \exp(-\lambda) \left[1 + \frac{T_{i\perp}}{T_{i\parallel}} \frac{Z'(\xi^M)}{2} \right], \quad (9)$$

where $\xi = i\gamma_k^M / k_{\parallel} v_{i\parallel}$. Like for the firehose instability, the terms of the order $(\omega_k / \omega_{pi})^2$ and ω_k / Ω_e were neglected in the dispersion relation for the ion-cyclotron and mirror modes.

The equations describing the evolution of the ion kinetic energy components are given by

$$n_i \frac{dT_{i\perp}}{dt} = -16\pi \int_0^\infty dk_{\parallel} \int_0^\infty k_{\perp} dk_{\perp} \times \left\{ \gamma_k^{IC} \frac{|\delta B_k^{IC}|^2}{8\pi} \left[1 + \left(\frac{\Re(\omega_k^{IC})}{\Omega_i} - \frac{1}{2} + \frac{\Lambda_1}{\lambda} \right) \frac{\Omega_i^2}{k^2 v_A^2} \right] + \gamma_k^M \frac{|\delta B_k^M|^2}{8\pi} \left[1 + \lambda (\Lambda_0 - \Lambda_1) \frac{\Omega_i^2}{k^2 v_A^2} \right] \right\}, \quad (10)$$

$$\begin{aligned} \frac{n_i}{2} \frac{dT_{i\parallel}}{dt} &= 8\pi \int_0^\infty dk_{\parallel} \int_0^\infty k_{\perp} dk_{\perp} \times \\ &\times \left\{ \gamma_{\mathbf{k}}^{IC} \frac{|\delta B_{\mathbf{k}}^{IC}|^2}{8\pi} \left[1 + 2 \left(\frac{\Re(\omega_{\mathbf{k}}^{IC})}{\Omega_i} - \frac{1}{2} + \frac{\Lambda_1}{\lambda} \right) \frac{\Omega_i^2}{k^2 v_A^2} \right] \right. \\ &\quad \left. + \gamma_{\mathbf{k}}^M \frac{|\delta B_{\mathbf{k}}^M|^2}{8\pi} \left[1 + 2\lambda (\Lambda_0 - \Lambda_1) \frac{\Omega_i^2}{k^2 v_A^2} \right] \right\}, \quad (11) \end{aligned}$$

where we used the definition $\Lambda_j = I_j(\lambda) \exp(-\lambda)$. The kinetic wave equations for the ion-cyclotron and mirror modes are

$$\frac{\partial |\delta B_{\mathbf{k}}^{IC}|^2}{\partial t} = 2\gamma_{\mathbf{k}}^{IC} |\delta B_{\mathbf{k}}^{IC}|^2. \quad (12)$$

$$\frac{\partial |\delta B_{\mathbf{k}}^M|^2}{\partial t} = 2\gamma_{\mathbf{k}}^M |\delta B_{\mathbf{k}}^M|^2. \quad (13)$$

The derivation of the above equations can be found in Yoon & Seough (2012).

4.3 Numerical methods

The quasilinear equations for the evolution of the ions temperature components and of the magnetic energy modes were integrated using the LSODE solver from the numerical library ODEPACK (Hindmarsh 1983; Radhakrishnan & Hindmarsh 1993). At each iteration, the linear dispersion equation for each instability is solved numerically inside a discrete domain $(k_{\parallel}(i), k_{\perp}(j))$ defined by $k_{\parallel,\perp}(i) = (i - 0.5) * k_{\max}/N$ ($1 \leq i \leq N$), where $0 < k_{\max} r_i < 2$, r_i is the thermal ion Larmor radius, and $N = 256$. For the firehose modes, only the unidimensional grid $k_{\parallel}(i)$ was used. For all the calculations presented, a flat spectrum of magnetic fluctuations $|\delta B_{\mathbf{k}}|^2/B_0^2 = 10^{-7}$ is imposed at the beginning of the simulation.

5 RESULTS

Top panel of Figure 1 shows the probability distribution function (PDF) of the macroscopic dimensionless plasma parameters $\beta_{i\parallel} = 8\pi n_i T_{i\parallel}/B^2$ and $A_i = T_{i\perp}/T_{i\parallel}$ for the CGL-MHD numerical simulation of forced turbulence described in Section 3 (i.e., model A2 of SL+14 with null scattering rate $\nu_S = 0$). Most of the plasma volume has the parameters $(\beta_{i\parallel}, A_i)$ inside the unstable zones. The thresholds for the mirror and firehose instabilities are represented in Figure 1 by the continuous gray lines and the threshold for the parallel ion-cyclotron (IC) instability is represented by the dashed gray line. We note that the threshold for the ion-cyclotron instability is more constraining than that of the mirror instability in the regime $\beta_{i\parallel} < 1$.

For a grid of values $(\beta_{i\parallel}, A_i)$ where the PDF of the CGL-MHD simulation is above an arbitrary cutoff of 10^{-7} (lighter gray dots in the bottom panel of Figure 1), we calculated the quasilinear evolution of the ion temperatures $T_{i\perp}$ and $T_{i\parallel}$ due to the wave-particle scattering of the ions by the parallel firehose, mirror, and ion-cyclotron modes. The evolved values of $(\beta_{i\parallel}, A_i)$ after a time interval $\Omega_i t = 500$ are shown as red dots in the bottom panel of Figure 1. For each initial condition, the plasma parameters evolved to values close to the marginal equilibrium state.

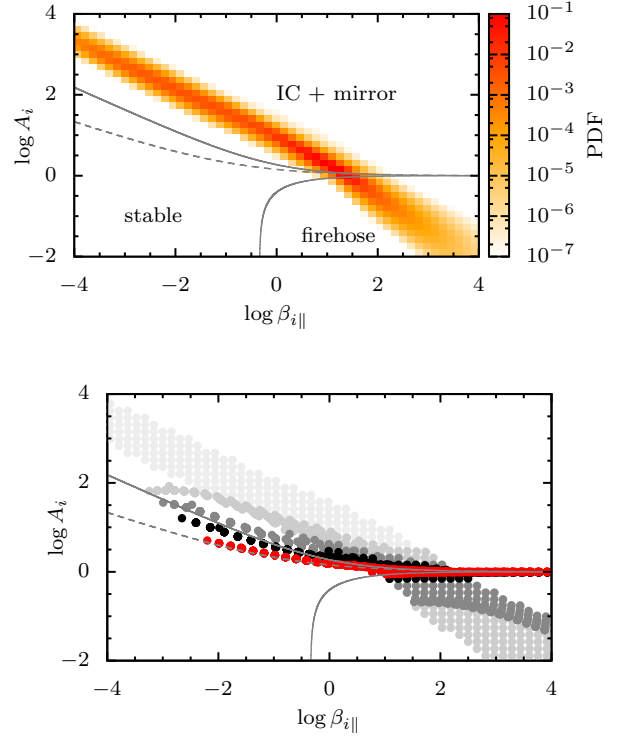


Figure 1. Top: probability distribution function (PDF) for the macroscopic plasma parameters $\beta_{i\parallel} = 8\pi n_i T_{i\parallel}/B^2$ and $A_i = T_{i\perp}/T_{i\parallel}$ obtained from the statistically stationary state of forced turbulence of the simulation using the CGL-MHD approximation by Santos-Lima et al. (2014, model A2 there). Bottom: initial values of $\beta_{i\parallel}$ and A_i from the quasilinear calculations (lighter gray dots) and values of the same parameters after the time interval $\Omega_i t = 500$ (red dots). The successively darker gray dots represent the system at the times $t = 10, 20, \text{ and } 40 \Omega_i^{-1}$. The gray solid lines represent the thresholds for the mirror $A_i = 1 + 0.87\beta_{i\parallel}^{-0.56}$ ($A_i > 1$) and parallel firehose $A_i = 1 - 0.61\beta_{i\parallel}^{-0.63}$ ($A_i < 1$) instabilities; the gray dashed line represents the threshold for the ion cyclotron (IC) instability $A_i = 1 + 0.43\beta_{i\perp}^{-0.42}$ (all the thresholds are obtained from linear theory; see Seough & Yoon 2012 and references therein).

Top panel of Figure 2 depicts the ions scattering rates $\langle \nu_S \rangle$ (normalized by the ion Larmor frequency Ω_i) resulting from the quasilinear evolution, as a function of the initial states $(\beta_{i\parallel}, A_i)$. These scattering rates were obtained from a temporal average of the instantaneous scattering rates, taking into account only values of $\nu_S \geq 0.6\nu_{\max}$, where ν_{\max} is the maximum scattering rate obtained during the time evolution. The values of $\langle \nu_S \rangle/\Omega_i$ are mostly in the interval $10^{-2} - 10^{-1}$, but inside the stable region they drop quickly to zero (this cannot be visualized in the Figure since the values of $\langle \nu_S \rangle$ fall below the color scale range at the region near $A_i \sim 1$). We further notice that the values of $\langle \nu_S \rangle/\Omega_i$ increase with $\beta_{i\parallel}$.

The bottom panel of Figure 2 shows, as a function of the initial states $(\beta_{i\parallel}, A_i)$, the maximum magnetic energy density in the modes (ion-cyclotron, mirror, and firehose) during the quasilinear evolution, normalized by the energy density of the background magnetic field B_0 . For most of the

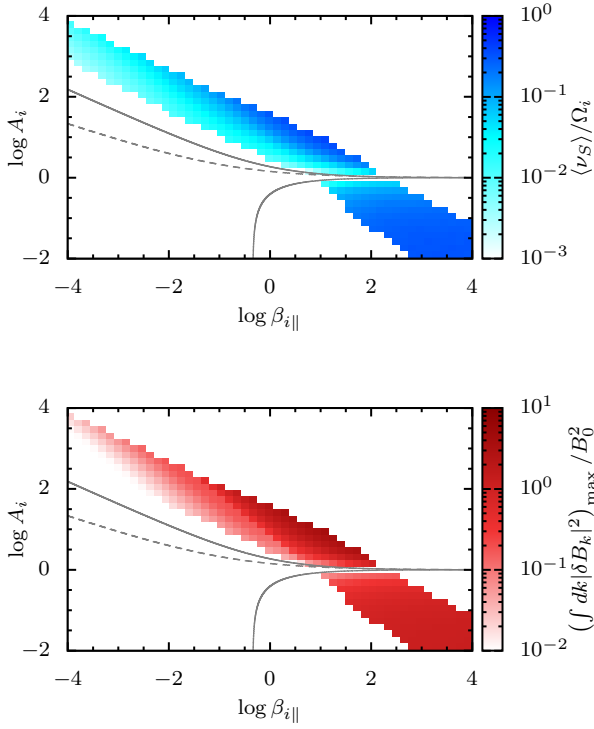


Figure 2. Top: ions scattering rate averaged in time $\langle \nu_S \rangle$ (normalized by the Larmor frequency Ω_i) for each initial state $(\beta_{i\parallel}, A_i)$ of the quasilinear evolution. The average in ν_S only considers times for which $\nu_S \geq 0.6\nu_{\max}$, where ν_{\max} is the maximum scattering rate during the system evolution. Bottom: maximum magnetic energy density in the ion-cyclotron + mirror ($A_i > 1$) and firehose ($A_i < 1$) modes during the quasilinear evolution of each initial state $(\beta_{i\parallel}, A_i)$. The gray lines have the same meaning as in Figure 1.

initial conditions, this quantity is below unity and does not break the assumption of small perturbations of the Larmor orbit. However, for initial conditions far from the thresholds (specially in the high- $\beta_{i\parallel}$ region for $A_i < 1$), it achieves values of the order or larger than 1. For this region, the values of $\langle \nu_S \rangle$ shown in the top panel of Figure 2 must be taken with caution (see Section 6.2). Nonetheless, these same initial conditions are not expected to be accessible by the ICM plasma if the wave-particle scattering is taken into account during the CGL-MHD evolution (see below).

Top panel of Figure 3 shows the characteristic rate of the anisotropy relaxation caused by the scattering due to the instabilities $\Gamma_\nu = |(\partial A_i / \partial t)_\nu| A_i^{-1}$ (normalized by the ion Larmor frequency Ω_i) as a function of the initial plasma parameters $(\beta_{i\parallel}, A_i)$, according to Eq. 3 and $\langle \nu_S \rangle$ from the quasilinear calculations. The characteristic rate at which the anisotropy changes in the CGL-MHD turbulence simulation described above, $\Gamma_A = |\langle \partial A_i / \partial t \rangle_{CGL}| A_i^{-1}$ (normalized by the ion Larmor frequency Ω_{i0} in the uniform magnetic field B_0 ; see Eq. 2), is shown in the bottom panel of Figure 3. The average in $\langle \partial A_i / \partial t \rangle_{CGL}$ considers only the plasma volume of the simulation with $(\partial A_i / \partial t)_{CGL} > 0$ when $A_i > 1$ and $(\partial A_i / \partial t)_{CGL} < 0$ when $A_i < 1$, in order to capture the rate

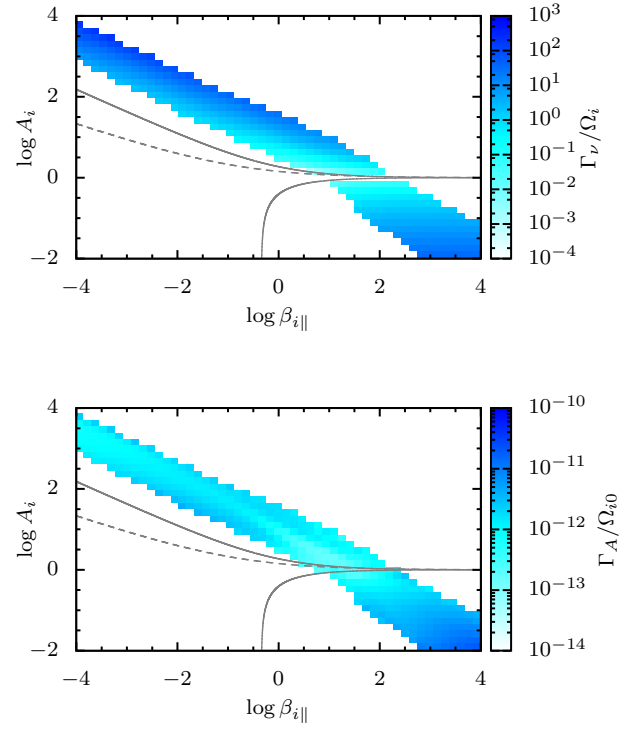


Figure 3. Top: characteristic rate of anisotropy relaxation (normalized by the proton Larmor frequency Ω_i) due to the instabilities scattering $\Gamma_\nu = |(\partial A_i / \partial t)_\nu| A_i^{-1}$ calculated using the average quasilinear scattering rates $\langle \nu_S \rangle$ (see Eq. 3). Bottom: characteristic rate of anisotropy increase (for $A_i > 1$) or decrease (for $A_i < 1$) obtained from the CGL-MHD turbulence simulation of Figure 1 (top), $\Gamma_A = |\langle \partial A_i / \partial t \rangle_{CGL}| A_i^{-1}$ normalized by the proton Larmor frequency Ω_{i0} of the mean magnetic field B_0 (see Eq. 2). The average was performed using only the plasma volume where the anisotropy A_i was increasing for $A_i > 1$ and decreasing for $A_i < 1$.

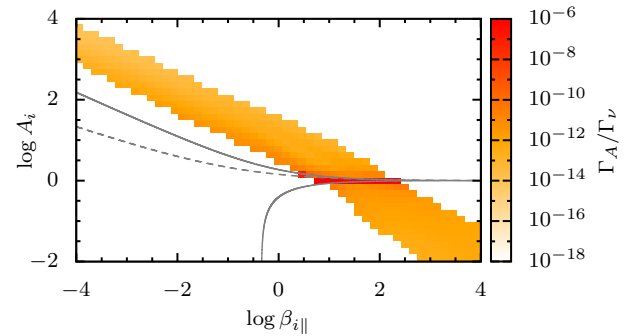


Figure 4. Ratio between the characteristic rate of anisotropy change obtained from the CGL-MHD turbulence simulation $\Gamma_A = |\langle \partial A_i / \partial t \rangle_{CGL}| A_i^{-1}$ and the characteristic rate of anisotropy relaxation calculated from quasilinear theory $\Gamma_\nu = |(\partial A_i / \partial t)_\nu| A_i^{-1}$ (both presented in Figure 3).

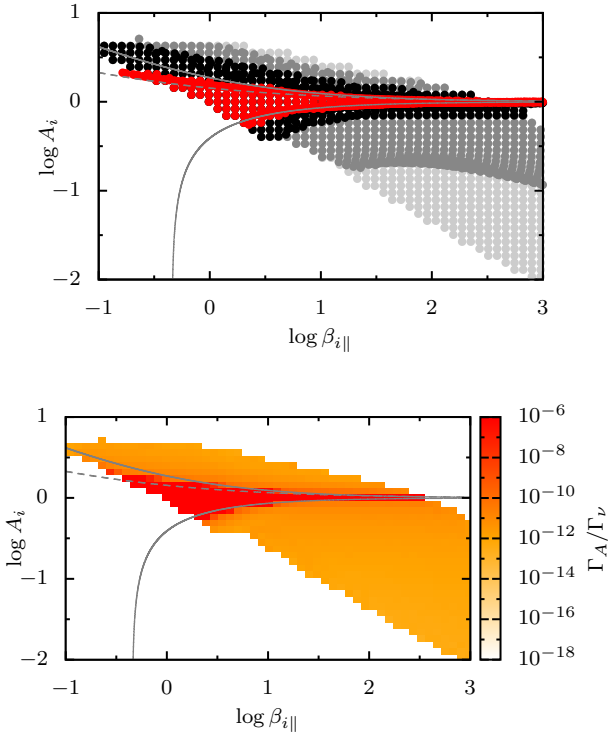


Figure 5. Top: same as Figure 1 (bottom panel), but using the initial values of $(\beta_{i\parallel}, A_i)$ obtained from a turbulence AMHD simulation which employed a non-null, constant rate ν_S in the equation of anisotropy evolution (model A3 of SL+14). Here the gray dots correspond to the times $t = 0, 20,$ and $40 \Omega_i^{-1}$ (from the lighter to the darker ones). Bottom: same as in Figure 4, but for the model above.

at which the anisotropy is driven apart from the stable zone. It is evident that $\Gamma_\nu \gg \Gamma_A$ for all the unstable region.³

It is clear that the maximum and minimum values of A_i that the turbulence can sustain are limited by the temperature anisotropy relaxation rates due to the instabilities. By comparing Γ_A and Γ_ν , we can find for each value of $\beta_{i\parallel}$ the maximum/minimum values of A_i (A_i^\pm) from the balancing $\Gamma_A(A_i^\pm) = \Gamma_\nu(A_i^\pm)$. Figure 4 shows the ratio Γ_A/Γ_ν between the rates presented in Figure 3. The separation of A_i^\pm from the mirror and firehose thresholds cannot be resolved for the grid in the $(\beta_{i\parallel}, A_i)$ -plane used in our calculations. However, it is evident that this separation is $\ll 1$. It shows that the turbulence can only sustain values of the temperature anisotropy A_i which are extremely close to the instabilities thresholds. Therefore the anisotropy levels featuring in the CGL-MHD simulation for the ICM turbulence are far from realistic.

We repeated all the above analysis, but now replacing the CGL-MHD simulated model used so far (model A2 of

SL+14 with null ν_S) for a simulated AMHD model in which a non-null constant value of ν_S was employed (model A3 of SL+14, with $\nu_S \sim 10 u_{rms}/l_{turb}$).

Figure 5 presents the evolution of $(\beta_{i\parallel}, A_i)$ (top panel), and the ratio between the anisotropy change rate $\Gamma_A = |(\partial A_i/\partial t)_{CGL}| A_i^{-1}$ and the characteristic rate of anisotropy relaxation $\Gamma_\nu = |(\partial A_i/\partial t)_\nu| A_i^{-1}$. The results of the quasi-linear evolution calculation are now similar to those of the simulated CGL-MHD turbulence model with the balancing between the rates Γ_A and Γ_ν very close to the thresholds for the instabilities.

6 DISCUSSION

6.1 Limitations of the CGL-MHD model to describe compressible modes

The CGL closure provides the simplest fluid model for a collisionless plasma, and assumes no heat flux. In particular, the linear dispersion of the CGL-MHD equations is known to deviate from the long wavelength limit of the kinetic theory for compressible modes, resulting in a different threshold for the mirror instability (being over-stable compared to the threshold obtained from the kinetic theory). Besides, for simplicity, we considered a CGL-MHD model with the same anisotropy in temperature and total thermal energy for both the ions (protons) and electrons (see discussion in SL+14 and below).

Another serious limitation of the CGL-MHD model is that it does not capture the collisionless damping effects of the compressible modes (see, e.g. Yan & Lazarian 2004). Alternative higher order closures exist which can mimic the Landau damping of the compressible modes, at least for a narrow range of wavelengths (see for example Snyder, Hammett, & Dorland 1997; Sharma et al. 2006). In view of this, we should be cautious with regard to compressible modes cascade (and shocks) in CGL-MHD based models.

The spatial scale in which the collisionless thermal damping may be dominant in the collisionless intracluster medium is ~ 0.1 -1 kpc (Brunetti & Lazarian 2007) and therefore well below of the approximate inertial range of the turbulent models discussed here (between 5 and 40 kpc). Thus a potential influence of the Landau damping in the models discussed here would be only in shock regions formed by the turbulence.

On the other hand, if a considerable reduction of the parallel ion mean free path is assumed to occur continuously in time in most of the plasma volume — via the scattering or magnetic trapping of the ions by the plasma instabilities (see next sections), this problem could be solved at least in part, because the large scale turbulence in the ICM would become effectively “collisional”. However, the knowledge of the spatial/temporal statistics of the parallel ions mean free path in the turbulent ICM is highly non-trivial, because the state of the micro-physical instabilities depends not only on the instantaneous properties of the flow and the macroscopic variables, but also on their evolution history (Melville, Schekochihin, & Kunz 2016; see also the discussion in the next sections).

³ However, the values of Γ_A from the simulations are expected to increase with resolution; the average value obtained in the simulation presented here could be until 6 orders of magnitude below the real one (see discussion in Section 6.4). Even taking into account this possible big difference, the inequality $\Gamma_\nu \gg \Gamma_A$ is still largely valid.

6.2 Limitations of the quasilinear theory applied to initially unstable plasma configurations

The quasilinear theory used here to calculate the evolution of the plasma instabilities arising from an initially unstable configuration has, of course, limitations, which are (at least in part) related to: (i) the linear approximations assumed, (ii) the assumption that the distribution function is bi-Maxwellian all the time, (iii) the neglect of non-linear interaction between waves, and specially (iv) the assumption of an homogeneous final state of plasma equilibrium.

Considering the limitation imposed by (i), it should be pointed out that although the quasilinear approximation is formally only applicable for very small perturbations, the thermal ions are not sensitive to perturbations much larger than their gyro-radius, which are generated also by the instabilities. Thus, the condition $\delta B^2/B_0^2 \ll 1$ can be slightly relaxed, considering the magnetic energy of the fluctuations $\propto \delta B^2$ integrated over all the spectrum.

Recently, [Seough, Yoon, & Hwang \(2014\)](#) performed one-dimensional Particle-In-Cell (PIC) simulations of the ion cyclotron instability for a limited set of initial conditions (with a fixed anisotropy $T_{i\perp}/T_{i\parallel} = 4$ and different values of $\beta_{i\parallel}$). They compared the evolution of the thermal energy components and of the total magnetic energy in the instabilities with the quasilinear predictions, finding good agreement for the moderate and high beta regimes ($\beta_{i\parallel} = 1$ and 10), for which the linear assumption $\delta B^2/B_0^2 \lesssim 1$ is maintained all the time. In the low beta regime ($\beta_{i\parallel} = 0.1$) however, the exponential growth of the instability ceased soon after the waves energy reached the background magnetic energy level (at $t \approx 50 \Omega_i^{-1}$), giving place to a nearly linear growth until the saturation. Nonetheless, the quasilinear predictions still provided a reasonable approximation to the PIC experiment in this case for the evolution of the thermal anisotropy. The authors also observed that the ions distribution function deviates from a bi-Maxwellian during the early stages of the instability evolution, but this deviation vanishes at late times when the system achieves the stationary, saturated state (after $\sim 100\Omega_i^{-1}$).

We have also carried out comparisons of the evolution of the instabilities obtained from two-dimensional hybrid simulations by [Gary, Yin, & Winske \(2000\)](#) for a plasma with dominant perpendicular temperature with quasilinear calculations taking into account both the oblique ion cyclotron and mirror modes (see the Appendix A). These results show good agreement (within an order of magnitude) between the scattering rates, specially for large values of the initial ion cyclotron growth rate. For the smallest values, the quasilinear scattering rates seem to overestimate the ones from the simulations.

On the other hand, it has been verified in two-dimensional PIC and hybrid simulations the dominance of the mirror modes (which are oblique to the background magnetic field) over the ion cyclotron modes for regimes of $\beta_{i\parallel} \gtrsim 1$, even when the ion cyclotron modes have growth rates comparable to the mirror modes ([Kunz, Schekochihin, & Stone 2014](#); [Riquelme, Quataert, & Verscharen 2015](#)). These last numerical experiments focused on the situation in which the thermal energy is initially isotropic and one component of the external magnetic field has its intensity changed at a constant rate (in a shear box configuration, represent-

ing the magnetic field shearing caused by the large scale MHD turbulence motions) driving in this way the increase of the perpendicular temperature (see Section 6.3). Also employing two-dimensional PIC simulations, [Sironi & Narayan \(2015\)](#) showed that the relative role of the mirror and ion cyclotron instabilities is dependent of the electron to ion temperature ratio T_e/T_i , being the ion cyclotron instability dominant only when $T_e/T_i \lesssim 0.2$ for high beta plasmas (for the studied range $\beta_i \sim 5 - 30$). Even in this situation, the mirror modes can dominate after one time-scale associated to the anisotropy driving rate. In the turbulent ICM, only a detailed modeling of the thermodynamical evolution of the species (taking into account electron-ion anomalous collisional processes) could provide the information on the local deviations from the thermal equilibrium between electrons and ions (see discussion in Section 6.4). With respect to the global ICM properties, [Takizawa \(1998, 1999\)](#) show that during the merger of sub-clusters of galaxies, the electrons temperature can be half of that of the ions in the post-shock ICM gas, in the outskirts of the cluster (where the electron-ion collision time is larger due to the lower density). However, these studies considered the thermal coupling between ions and electrons mediated by Coulomb collisions only, and did not include any magnetic fields.

A detailed study comparing fully non-linear plasma simulations with a quasilinear approximation is still missing for the mirror instability. However, the stabilization mechanism of the mirror instability can be very different depending on the initial conditions of the temperature anisotropy. Very large anisotropies could produce modes with wavelengths close to the ion Larmor radius, in the case when the irreversible ions scattering is likely to drive the system to the marginal stability. However, these required levels of anisotropy can be artificially high, like the ones generated by the CGL-MHD turbulence presented in this work. In this scenario, the quasilinear scattering rates calculated here may be considered as a “zeroth” order approximation.

For moderate values of the anisotropy beyond the threshold, the saturated state of the mirror instability can be achieved by highly inhomogeneous and stable configuration of the plasma and magnetic field ([Kivelson & Southwood 1996](#)), without breaking the magnetic momentum of the ions via anomalous scattering. The total pressure equilibrium can be achieved by the betatron cooling of the trapped protons only ([Pantellini 1998](#)).

Now lets us focus our attention on the plasma regime in which the parallel temperature is dominant and therefore, the firehose instability is present. [Seough, Yoon, & Hwang \(2015\)](#) compared directly the quasilinear evolution of the parallel firehose instability with one-dimensional PIC simulations with fixed initial anisotropy $T_{i\perp}/T_{i\parallel} = 0.1$ and different values of the plasma beta parameter: $\beta_{i\parallel} = 2.5, 5, \text{ and } 10$. Similar to the ion cyclotron study ([Seough, Yoon, & Hwang 2014](#)), the quasilinear predictions provide a better agreement for the highest values of $\beta_{i\parallel}$. However, after a short initial phase of exponential growth where the quasilinear calculations are almost identical to the simulations, the saturation values of the magnetic energy modes predicted by the quasilinear calculations are found to be larger than the values obtained from the plasma simulations. For the lowest value of $\beta_{i\parallel}$ tested ($\beta_{i\parallel} = 2.5$), the agreement is the poorest and the final saturated value of the

anisotropy is far from the threshold of the firehose instability. They also observed that the deviation from the initial bi-Maxwellian velocity distribution is larger for smaller $\beta_{i\parallel}$. The authors suggest that the existence of strong wave-wave interactions could be responsible for the deviation from the quasilinear calculations.

The quasilinear calculations presented in this study only consider the evolution of the plasma instabilities from a set of initially unstable plasma configurations taken from the statistics of numerical simulations of CGL-MHD turbulence that did not consider self-consistently the feedback of the small-scale (subgrid) plasma instabilities. If our quasilinear rates of anisotropy relaxation due to the ions scattering are valid at least in order of magnitude, the straightforward conclusion that one can draw is that there is an obvious physical inconsistency in neglecting the micro-instabilities effects on the evolution of the temperature anisotropy in anisotropic MHD (AMHD) simulations of turbulence, at least for the observed conditions of the ICM. Even for an AMHD model with an imposed anisotropy relaxation rate of $\nu_{\text{eff}} \approx 10\tau_{\text{turb}}^{-1}$ (where τ_{turb} is the turbulence turn-over time) is uniform over all the firehose and mirror unstable volume, the levels of temperature anisotropy achieved would generate micro-instabilities so strong in a real plasma that they would bring the anisotropy to the (near) marginal state almost “instantaneously” (\sim ion kinetic time-scales).

6.3 Mirror and firehose development under slow temperature anisotropy driving

Recent kinetic simulations have shed some light on the saturation mechanism of the mirror and firehose instabilities in the context of “slow” anisotropy driving, as expected by the ICM turbulence. Kunz, Schekochihin, & Stone (2014) examines the development of the mirror and firehose instabilities in the situation where the anisotropy is continuously driven at a nearly linear rate $S \sim A^{-1} |(\partial A / \partial t)_{\text{CGL}}| \ll \Omega_i$ (see Eq. 2) by the large scale shear of the background magnetic field. Riquelme, Quataert, & Verscharen (2015) did a similar study for the mirror instability only. Both studies focus on the regime of $\beta \approx 200$, characteristic of ICM conditions. Melville, Schekochihin, & Kunz (2016) extends these studies to higher values of β (relevant for the problem of magnetic field amplification in the ICM), and also analyses the decaying/evolution of the instabilities when the anisotropy driving ceases or is reverted.⁴

These studies clearly show that the temperature anisotropy is tightly limited by the firehose and mirror marginal stability thresholds in the asymptotic limit $S \ll \Omega_i$. For the firehose instability, in the regime $(S\beta/\Omega_i) \ll 1$ (relevant for the ICM parameters), the anomalous scattering is set by the macroscopic anisotropy generation rate S after a time delay $\delta t \ll S^{-1}$, while in the regime when $(S\beta/\Omega_i) \gtrsim 1$ (relevant for the early scenario of magnetic field amplification in the ICM), the time interval δt for the development of the magnetic fluctuations able to scatter the ions at a rate which equilibrates the anisotropy

generation is $\delta t \gtrsim S^{-1}$ (Kunz, Schekochihin, & Stone 2014; Melville, Schekochihin, & Kunz 2016). In both cases, the firehose fluctuations decay exponentially at a rate $\sim \Omega_i/\beta$ after the shutdown of the anisotropy driving (Melville, Schekochihin, & Kunz 2016). In contrast, for mirror instability the magnetic fluctuations keep increasing continuously during all the shear time S^{-1} , with the maintenance of the marginal stability condition due to the increasing fraction of ions trapped in regions where the increase of the magnetic field is compensated by the magnetic fluctuations (the trapped particles do not feel the increase of the mean magnetic field and are not subject to betatron acceleration; see Kunz, Schekochihin, & Stone 2014; Riquelme, Quataert, & Verscharen 2015; Rincon, Schekochihin, & Cowley 2015). These magnetic structures have $\delta B_{\parallel} \gg \delta B_{\perp}$ and are elongated in the direction of the local mean magnetic field. In the situation when the anisotropy driving is removed at $St = 1$, the mirror fluctuations decay at a rate $\sim \Omega_i/\beta$, slower than exponential (Melville, Schekochihin, & Kunz 2016).

Melville, Schekochihin, & Kunz (2016) also analysed the situation when the direction of the anisotropy driving is reversed after the time S^{-1} . The firehose development on the top of the reminiscent mirror modes proceeds very similar to its development from the homogeneous and isotropic initial condition. In the case when the driving of excess of parallel pressure is inverted to an excess of perpendicular pressure, the plasma only develops enough anisotropy to trigger mirror modes after a substantial decaying of the firehose modes.

In the next section we further discuss our results in the light of those above, putting our work in a broader context.

6.4 Applicability of the bounded anisotropy model to turbulence simulations of the ICM

The physical fields evolved in our AMHD simulations of the ICM are in fact *mean fields*, in the sense that they represent macroscopic averages in space and time, over scales much larger than those related to the firehose and mirror modes expected to develop there. This macroscopic description therefore filters the “microscale” magnetic fluctuations which can achieve intensities comparable to the macroscopic magnetic field (for example, the firehose modes in the “ultra-high” beta regime⁵ described in Melville, Schekochihin, & Kunz 2016).

The most obvious complication of this description is related to the evolution of the macroscopic pressure components relative to the direction of the macroscopic magnetic field. For example, the development of a microscale transverse magnetic field component does not change the direction (or intensity) of the mean magnetic field. But it modifies the direction of the magnetic field in the small scales and at least part of the parallel pressure (with respect the microscopic local magnetic field) should contribute to increase the macroscopic perpendicular pressure. Also the changes in

⁴ The local shear rate $S \sim \delta v_{\perp}/l$ produced by turbulence in the scale l is expected to be coherent during the cascading time of these scales $\sim l/\delta v_{\perp} \sim S^{-1}$.

⁵ The “moderate” and “ultra-high” β regimes (respectively $\beta \ll \Omega_i/S$ and $\beta \gtrsim \Omega_i/S$ are defined in Melville, Schekochihin, & Kunz (2016), where the estimates for the critical β in the ICM turbulence are provided: $\beta_c \sim 10^{7-9}$, corresponding to magnetic field intensities $\sim 10^{-9} - 10^{-8}$ G.

the magnetic field intensity due to the microscopic components should produce changes in the macroscopic pressure anisotropy. In other words, the macroscopically seen thermal anisotropy *is* influenced by the development of microscale magnetic field fluctuations, even assuming the perfect conservation of the particles magnetic moment and excluding any kinetic effect. Summarizing, in the presence of micro-instabilities, the CGL closure for the mean, large scale fields is at least incomplete, as the microscopic effects eventually modify macroscopic thermal anisotropy evolution. Therefore, the inclusion of a “subgrid” model for the evolution of anisotropy in the AMHD description of the ICM turbulence is needed even in the absence of any irreversible scattering of the particles.

Another complication is that anisotropy generation rate by turbulence increases inversely to the scale of the motions: $\Gamma_A = A^{-1} |(\partial A / \partial t)_{CGL}| \sim d \ln B / dt \sim l^{-2/3}$ or $l_{\perp}^{-1/3}$ (considering the fast or Alfvénic/slow scaling for the velocity gradients; see [Yan & Lazarian 2011](#)). This means that the statistics of the anisotropy driving rate is strongly dependent on the inertial range of the simulation, and therefore, on the numerical resolution. In this way, considering the dominant scale for the anisotropy generation rate as the lowest scale of the inertial range of our simulations ($\sim 10^{22}$ cm), and using the power law corresponding to the Alfvénic/slow velocity gradients to extend it to the ions kinetic scales $\sim 10^5$ km, the average value of Γ_A from our simulations could increase by a factor of at most $\sim 10^4$.

To modify the CGL closure by imposing “hard wall” limits on the pressure anisotropy ([Sharma et al. 2006](#)) in the AMHD description of the ICM is equivalent to assume that the relaxation of the macroscopic anisotropy to the instabilities threshold happens in a timescale negligible compared to the macroscopic time scales. This assumption is well justified for both firehose and mirror instabilities, whenever the rate of anisotropy generation S is much smaller than the ion Larmor frequency Ω_i (see discussions in Sections 6.2 and 6.3), independent on the development of pitch angle scattering of the ions. However, it also assumes that the free-energy released by the instabilities, which (at least in part) would be stored in microscopic magnetic fluctuations, is directly converted into internal energy irreversibly. Firstly, in the case where the instabilities scatter the ions almost “instantaneously” during the anisotropy driving period, not necessarily all the free energy of the instability is transferred to the ions (or is equally distributed between ions and electrons), as some part of the electromagnetic energy cascades to the scales below the ion Larmor radius (see [Kunz, Schekochihin, & Stone 2014](#)) and ends up being transferred to the electrons. In any case, in the absence of a detailed description of the micro-turbulence cascading and of the full thermodynamics including ion-electron collision rates, emission/cooling processes for each specie, electrons acceleration etc, it is not meaningful to pursue such detailed energy distribution in AMHD simulations of the ICM (in the SL+14 simulations, thermal equipartition is assumed between the ion and electrons). Secondly, “removing” instantaneously the energy from the microscale magnetic fluctuations causes the magnetic energy pressure to be underestimated. However, the largest values of the relative magnetic energy of the fluctuations $\delta B^2 / B^2$ are of the order of unity ([Kunz, Schekochihin, & Stone 2014](#);

[Melville, Schekochihin, & Kunz 2016](#)), and as the thermal β values relevant for the ICM are high, the magnetic field pressure is secondary (compared to the thermal pressure) and also dynamically unimportant in the large scales (specially in the dynamo context). But it could also affect the detailed energy distribution between the species if radiative emission would to be taken into account. After the anisotropy driving ceases, the microscopic magnetic fluctuations decay at a rate regulated by the scattering of the ions ([Melville, Schekochihin, & Kunz 2016](#)). The magnetic energy of the fluctuations gradually released is not converted again in free energy of the thermal anisotropy thanks to the irreversible scattering of the ions. As discussed in the previous sections, the mirror and firehose magnetic fluctuations decay in a time scale relatively short after ceased the anisotropy driving, for moderate values of β . In the “ultra-high” β regime, however, these magnetic fluctuations persist during dynamical time-scales. This means that the bounded anisotropy model also cannot describe correctly the entropy evolution of the plasma.

To what extent could the ion scattering rate (and consequently the ions parallel mean free-path) be derived from the AMHD simulations of the turbulent ICM? Let us forget for a moment the complexity arising from the fact that the statistics (spatial and temporal) of the turbulent shearing/compression rates may depend on the micro-instabilities state (and on the resolution of the simulation, as discussed above), and assume that the statistics of the shearing/compression is known. As discussed before, for values of beta representative of the ICM, the firehose fluctuations instantaneously spark ions scattering at a rate needed to keep the macroscopic anisotropy at the marginal threshold level, making it possible to derive the statistics of the scattering. For the mirror modes (and also for the firehose modes in the regime of “ultra-high” beta), however, the determination of the scattering rate depends on the knowledge of the microscopic magnetic fluctuations level that develops during the macroscopic time-scales of the shear/compressions. It means that the macroscopic fields of the plasma cannot determine the local scattering rate at a given time.

Now we consider again the influences of the ions scattering rate on the AMHD turbulence evolution itself. In the absence of a significant decrease of the parallel mean free path of the ions, a strong collisionless damping of the compressible modes propagating parallel to the local field can be expected. However, the shear velocities of the Alfvén modes, transverse to the local magnetic field, are not expected to be affected by the ions parallel mean-free-path. That is, an MHD-like Alfvénic cascade is expected to develop independent of the ions parallel viscosity (see [Schekochihin et al. 2005](#)). The linear Alfvén modes are expected to be affected only by the shear viscosity component. Both the Braginskii shear viscosity $\sim r_i^2 \nu_{ii}$ (where r_i is the thermal ion Larmor radius and ν_{ii} the ion-ion collision rate) and the Landau damping cannot set a viscous scale for the Alfvénic strong cascade above the ion Larmor radius in the ICM regime of high beta plasma, subsonic turbulence (see a detailed discussion on this subject in [Borovsky & Gary 2009](#)). On the other hand, the compressible cascade will be damped already in the much larger scales. This damping is of kinetic origin, and its physics cannot be captured in AMHD simulations (see Section 6.1).

Conjecturing that the coupling between the compressible and Alfvénic modes in the anisotropic MHD is similar to that in isotropic pressure MHD (Cho & Lazarian 2003; Kowal & Lazarian 2010), the Alfvénic cascade must be energetically more important and little affected by the compressible cascade in the ICM. Therefore, the macroscopic turbulence statistics of the ICM should be well represented by the bounded anisotropy AMHD simulations if the precise thermodynamic description is not important.

However, in the absence of significant anomalous scattering of the ions (as it is expected in the “ultra-high” beta regime; see Melville, Schekochihin, & Kunz 2016), the micro-instabilities mechanism that will keep the pressure anisotropy limited is the suppression of the stretching rate of the magnetic field (Mogavero & Schekochihin 2014). This means that the velocity and magnetic fields from the micro-instabilities can affect the global stretching rate of the magnetic field, and therefore, the small scale dynamo evolution. In this scenario, the mirror instabilities, for example, could slow down considerably the turbulent amplification of the large scale magnetic field — but the situation is more complex because the persistent firehose fluctuations can suppress the development of the mirror modes (Melville, Schekochihin, & Kunz 2016). Such contribution from the microscales to the induction equation cannot be included easily in fluid simulations and hence, the results of the magnetic field amplification obtained from both in isotropic pressure MHD or bounded anisotropy AMHD previous simulations (e.g. SL+14) should be taken with caution, at least in regimes of very high beta (see more details on this subject in Mogavero & Schekochihin 2014; Melville, Schekochihin, & Kunz 2016).

It is worth to emphasize that several aspects of the ICM thermodynamics — like entropy generation (Lyutikov 2007), ion heat conduction (Kunz et al. 2011), physics of the compressible modes (see Section 6.1), etc. — which can have crucial importance for the ICM structuring and dynamics cannot be self-consistently approached by the boundary anisotropy AMHD model without a detailed modeling of the micro-instabilities evolution (Melville, Schekochihin, & Kunz 2016).

6.5 Implications to particle acceleration in the ICM turbulence

As discussed in Section 6.4, a modification of the CGL-MHD equations is required to account for the limits on the temperature anisotropy imposed by the thresholds of the instabilities firehose, mirror, and possibly ion cyclotron (in regions of low β) in studies of the turbulent ICM. In SL+14, such limits (mirror and firehose) were shown to bring the turbulence statistics to be similar to the collisional MHD counterpart, and the turbulent dynamo was also found to amplify the magnetic fields at rates compatible with those of the collisional MHD (neglecting the effects of the suppression of the stretching rate of the magnetic field by the micro-instabilities, see §6.4).

If the scattering and trapping of the ions by the instabilities makes the effective collisional scale of the thermal particles much smaller than the Coulomb ion-ion parallel collision scale over a significant fraction of the plasma, it could justify a drastic reduction of the collisionless damping

of the compressible modes by the thermal plasma. Invoking such a picture, Brunetti & Lazarian (2011) showed that the compressible modes can channel energy to re-accelerate efficiently relativistic particles in the ICM. In the absence of such anomalous scattering, only ten percent of the energy in the fast modes is available to accelerate the particles (Petrosian, Yan, & Lazarian 2006; Brunetti & Lazarian 2007).

However, as discussed in Section 6.3, a knowledge of the magnetic fluctuation level of the micro-scale mirror modes (and also of the firehose modes in the “ultra-high” beta regime; see Footnote 5) is required in order to make an estimative of the trapped fraction and scattering rate of the ions. In fact, as the evolution of the mirror modes occurs during the macroscopic time scales, the ions parallel mean free path will reduce gradually in time in the spatial location where the turbulence drives the anisotropy generation. Localized (in space and time) reduction of the ions mean free path in the turbulent plasma should be expected, but a detailed statistics (spatial/temporal distribution) in connection with the turbulence cascade is necessary to understand its impact on the damping of the compressible modes. This question deserves further extensive investigation.

7 SUMMARY AND CONCLUSIONS

Previous numerical simulations of forced turbulence representing the intracluster medium regime showed that the turbulence can produce very high levels of anisotropy in the temperature when the plasma instabilities feedback is neglected (SL+14). This anisotropy has an important impact on the turbulence statistics, producing significant modifications when compared to one-temperature collisional MHD turbulence (see also Nakwacki et al. 2016 for a study on the impact of the pressure anisotropy on the Faraday rotation maps of the ICM). It also prevents the turbulent amplification of the magnetic fields, which is believed to be responsible for sustaining the observed intensities and coherence lengths of the magnetic fields present in the ICM (Kotarba et al. 2011; Egan et al. 2016).

Using a grid of different initial conditions ($\beta_{i\parallel}, A_i$) taken from a distribution produced by a CGL-MHD simulation, we calculated the non-linear evolution of the ions temperature components due to the pitch-angle scattering caused by the plasma mirror, ion-cyclotron, and parallel firehose instabilities using the quasilinear theory where we assumed an isotropic distribution for the electrons temperature. The quasilinear evolution brings the values of ($\beta_{i\parallel}, A_i$) close to the limits of marginal stability after a few hundred ion Larmor periods.

In counterpart, we computed the average rate at which the simulated CGL-MHD turbulence pushes the temperature anisotropy in the direction of unstable values. We showed that this rate is several orders of magnitude smaller than the rate at which the pitch-angle scattering by the instabilities drives the temperature anisotropy towards the stable values, even when starting with small deviations from the instabilities thresholds. The quasilinear evolution of the ions temperature anisotropy used here was also compared to that obtained from two-dimensional hybrid simulations for a small set of unstable initial conditions in which the plasma

develops ion-cyclotron modes. This comparison shows good accordance (within an order of magnitude) for the rate of pitch-angle scattering (see Appendix A).

Our quasilinear analysis demonstrates clearly that in the turbulent ICM, the fast scattering of the ions by the instabilities rules out the presence of temperature anisotropies levels exceeding substantially the thresholds for the instabilities. When the anisotropy level is very close to the threshold of the instabilities, the slow instability growth favors adiabatic evolution to the saturation, and then the quasilinear scattering rates may become less representative (see Section 6.2 and 6.3). The last observation is particularly relevant in the case of the mirror instability.

Additionally, the development of the instabilities should take into account the continuous anisotropy driving during the macroscopic turbulence time scales. Such problem was recently addressed in the studies by Kunz, Schekochihin, & Stone (2014), Riquelme, Quataert, & Verscharen (2015), and Melville, Schekochihin, & Kunz (2016), with the conclusion that the instabilities induced by the ICM turbulence indeed keep the thermal anisotropy bounded by the instabilities thresholds during all the relevant macroscopic time-scales. The scattering rate of the ions is set “instantaneously” (for the macroscopic time-scales) by the firehose instability, and it is responsible for the anisotropy relaxation which keeps the anisotropy limited. But this is not the case regarding the mirror instability, for which the ions scattering increases gradually during the time-scale of the anisotropy generation by the turbulence shear/compression. In this case, the anisotropy is limited to the thresholds by processes essentially adiabatic (at least initially).

In conclusion, all these results and considerations justify the modification of the CGL-MHD equations for including bounds of the anisotropy at the instabilities thresholds, which is appropriate for the description of the ICM turbulence. As the anisotropy relaxation rate derived from these bounds does not necessarily reflect the instantaneous scattering rate of the ions by the instabilities (at least for the mirror modes), such bounded anisotropy models cannot represent properly the thermodynamical evolution of the gas nor the damping of the compressible modes, which depend on the parallel ions mean-free-path. Even considering these limitations (see Section 6.4), the bounded anisotropy model should represent well the Alfvénic cascade of the turbulence, assuming that thermodynamical details play no major role in the turbulence dynamics. It has been shown in the earlier study of SL+14 that if the temperature anisotropy is bounded to stable values (considering only the mirror and firehose instabilities), the turbulence statistics and the magnetic field amplification due to the small-scale dynamo have results undistinguishable from the one-temperature MHD description largely used in studies of the intracluster medium. We note however, that this last study did not take into account the potential effects of the microscale instabilities on the stretching rate of the magnetic field during the turbulent amplification which can be important at least in very high beta regimes (Section 6.4).

Finally it should be emphasized that any phenomenon depending on the ion thermal parallel mean-free-path which can affect the intracluster medium structuring (e.g., via heat conduction, thermal instabilities, cooling), and also cosmic-

ray acceleration (see Section 6.5) deserve still further investigation considering the complex interplay between the macroscopic turbulence and the detailed evolution of the microscopic instabilities.

ACKNOWLEDGEMENTS

RSL acknowledges partial support from a grant of the Brazilian Agency FAPESP (2013/15115-8). RSL and HY acknowledge the support by NSFC11473006 for RSL’s first visit to HY, during which part of this work was developed. EMGDP acknowledges partial support from FAPESP (2013/10559-5) and CNPq (306598/2009-4) grants. AL acknowledges the NSF grant AST 1212096 and Center for Magnetic Self Organization (CMSO) as well as a distinguished visitor PVE/CAPES appointment at the Physics Graduate Program of the Federal University of Rio Grande do Norte and thanks the INCT INEspaço. RSL also thanks the kind hospitality of the Astronomy department of the University of Wisconsin/Madison where part of this work was developed. RSL and EMGDP are indebted to D. Falceta-Gonçalves for useful discussions on plasma physics, and M. Kunz for the insightful discussions on the plasma instabilities evolution. The authors are indebted to an anonymous referee for pointing out some misconceptions in the original manuscript and for providing important suggestions to improve this work.

REFERENCES

- Bale S. D., Kasper J. C., Howes G. G., Quataert E., Salem C., Sundkvist D., 2009, *PhRvL*, 103, 211101
- Borovsky J. E., Gary S. P., 2009, *PhPl*, 16, 082307
- Brunetti G., Lazarian A., 2011, *MNRAS*, 412, 817
- Brunetti G., Lazarian A., 2007, *MNRAS*, 378, 245
- Chew G. F., Goldberger M. L., Low F. E., 1956, *RSPSA*, 236, 112
- Cho J., Lazarian A., 2003, *MNRAS*, 345, 325
- Egan H., O’Shea B. W., Hallman E., Burns J., Xu H., Collins D., Li H., Norman M. L., 2016, arXiv:1601.05083
- Falceta-Gonçalves D., Kowal G., 2015, *ApJ*, 808, 65
- Gary S. P., 1993, *tspm.book*, 193
- Gary S. P., Li H., O’Rourke S., Winske D., 1998, *JGR*, 103, 14567
- Gary S. P., Wang J., Winske D., Fuselier S. A., 1997, *JGR*, 102, 27159
- Gary S. P., Yin L., Winske D., 2000, *GeoRL*, 27, 2457
- Hau L.-N., Wang B.-J., 2007, *NPGeo*, 14, 557
- Hellinger P., Passot T., Sulem P.-L., Trávníček P. M., 2013, *PhPl*, 20, 122306
- Hellinger P., Trávníček P., Kasper J. C., Lazarus A. J., 2006, *GeoRL*, 33, L09101
- Hindmarsh A. C., “ODEPACK, A Systematized Collection of ODE Solvers,” in *Scientific Computing*, R. S. Stepleman et al. (eds.), North-Holland, Amsterdam, 1983 (vol. 1 of *IMACS Transactions on Scientific Computation*), pp. 55-64
- Keiter P. A., 1999, *PhDT*, 5389
- Kivelson M. G., Southwood D. J., 1996, *JGR*, 101, 17365
- Kotarba H., Lesch H., Dolag K., Naab T., Johansson P. H., Donnerert J., Stasyszyn F. A., 2011, *MNRAS*, 415, 3189
- Kowal G., Falceta-Gonçalves D. A., Lazarian A., 2011, *NJPh*, 13, 053001
- Kowal G., Lazarian A., 2010, *ApJ*, 720, 742
- Kunz M. W., Schekochihin A. A., Cowley S. C., Binney J. J., Sanders J. S., 2011, *MNRAS*, 410, 2446

- Kunz M. W., Schekochihin A. A., Stone J. M., 2014, PhRvL, 112, 205003
- Lazarian A., Beresnyak A., 2006, MNRAS, 373, 1195
- Le A., Egedal J., Fox W., Katz N., Vrublevskis A., Daughton W., Drake J. F., 2010, PhPl, 17, 055703
- Lyutikov M., 2007, ApJ, 668, L1
- Marsch E., 2006, LRSP, 3,
- Maruca B. A., Kasper J. C., Gary S. P., 2012, ApJ, 748, 137
- Melville S., Schekochihin A. A., Kunz M. W., 2016, MNRAS,
- Meng X., Tóth G., Liemohn M. W., Gombosi T. I., Runov A., 2012, JGRA, 117, A08216
- Mogavero F., Schekochihin A. A., 2014, MNRAS, 440, 3226
- Nakwacki M. S., Kowal G., Santos-Lima R., de Gouveia Dal Pino E. M., Falceta-Gonçalves D. A., 2016, MNRAS, 455, 3702
- Nakwacki M. S., Peralta-Ramos J., 2013, arXiv, arXiv:1312.7822
- Nishimura K., Gary S. P., Li H., 2002, JGRA, 107, 1375
- Pantellini F. G. E., 1998, JGR, 103, 4789
- Petrosian V., Yan H., Lazarian A., 2006, ApJ, 644, 603
- Radhakrishnan K., Hindmarsh A. C., "Description and Use of LSODE, the Livermore Solver for Ordinary Differential Equations," LLNL report UCRL-ID-113855, December 1993
- Rincon F., Schekochihin A. A., Cowley S. C., 2015, MNRAS, 447, L45
- Riquelme M. A., Quataert E., Sharma P., Spitkovsky A., 2012, ApJ, 755, 50
- Riquelme M. A., Quataert E., Verscharen D., 2015, ApJ, 800, 27
- Santos-Lima R., de Gouveia Dal Pino E. M., Kowal G., Falceta-Gonçalves D., Lazarian A., Nakwacki M. S., 2014, ApJ, 781, 84
- Schekochihin A. A., Cowley S. C., 2006, PhPl, 13, 056501
- Schekochihin A. A., Cowley S. C., Kulsrud R. M., Hammett G. W., Sharma P., 2005, ApJ, 629, 139
- Seough J., Yoon P. H., 2012, JGRA, 117, A08101
- Seough J., Yoon P. H., Hwang J., 2015, PhPl, 22, 012303
- Seough J., Yoon P. H., Hwang J., 2014, PhPl, 21, 062118
- Sharma P., Hammett G. W., Quataert E., Stone J. M., 2006, ApJ, 637, 952
- Sironi L., 2015, ApJ, 800, 89
- Sironi L., Narayan R., 2015, ApJ, 800, 88
- Snyder P. B., Hammett G. W., Dorland W., 1997, PhPl, 4, 3974
- Štverák Š., Trávníček P., Maksimovic M., Marsch E., Fazakerley A. N., Scime E. E., 2008, JGRA, 113, A03103
- Tajima T., Mima K., Dawson J. M., 1977, PhRvL, 39, 201
- Takizawa M., 1999, ApJ, 520, 514
- Takizawa M., 1998, ApJ, 509, 579
- Tanaka M., 1993, JCoPh, 107, 124
- Yan H., Lazarian A., 2011, ApJ, 731, 35
- Yan H., Lazarian A., 2004, ApJ, 614, 757
- Yan H., Lazarian A., 2002, PhRvL, 89, 281102
- Yoon P. H., Seough J., 2012, JGRA, 117, A08102

APPENDIX A: QUASILINEAR EVOLUTION OF THE ION-CYCLOTRON INSTABILITY COMPARED TO PLASMA SIMULATION

We present here a comparison between the evolution of the temperature anisotropy obtained from two-dimensional hybrid simulations presented in Gary, Yin, & Winske (2000, G+00 hereafter), and our quasilinear approach described in Section 4.

We have evolved the ions temperature components and the magnetic field waves energy, using equations 10 to 13, for a set of initial values of $\beta_{i\parallel}$ and $A_i = T_{i\perp}/T_{i\parallel}$ similar to those employed in G+00. We considered an initial flat spectrum for the magnetic waves with $|\delta B_{\mathbf{k}}|^2/B_0^2 = 10^{-7}$.

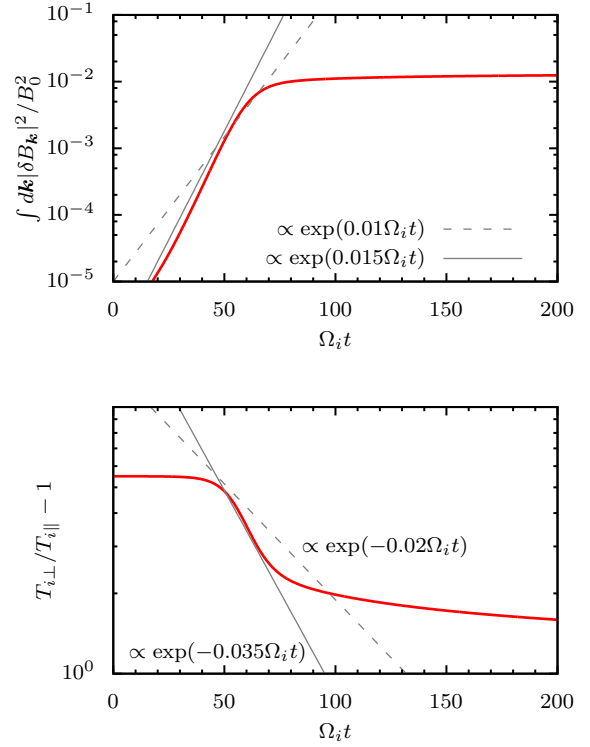


Figure A1. Temporal evolution of the magnetic energy density perturbations (top) and temperature anisotropy (bottom). The initial conditions are $\beta_{i\parallel} = 0.05$ and $T_{i\perp}/T_{i\parallel} = 6.5$. The dashed gray lines represent the fitting presented in Gary, Yin, & Winske (2000) for the 2D hybrid simulations with similar initial conditions. The continuous gray lines represent the curves which are the best fitting to the present quasilinear results (see text).

Figure A1 shows the evolution of the energy density of the magnetic fluctuations $W_B = \int dk |\delta B_{\mathbf{k}}|^2 / B_0^2$ (top panel), and the evolution of the ions temperature anisotropy (bottom panel) for one particular initial condition: $\beta_{i\parallel} = 0.05$ and $A_i = 6.5$. This evolution is qualitatively similar to that obtained from the 2D hybrid simulation of G+00 (see their Figure 1). After a short time interval, W_B increases exponentially. The particles scattering due to these magnetic fluctuations modifies the ions thermal velocity distribution and leads to a fast decrease in the anisotropy at the same time that the magnetic fluctuations grow very fast (bottom panel of Figure A1). The anisotropy in temperature decreases exponentially during this time interval. After this phase, it continues to decrease but at a slower rate.

Figure A2 shows for the complete set of the quasilinear calculations the maximum values of the energy density of the magnetic fluctuations (top panel), the initial (blue triangles) and final (red squares) values of the temperature anisotropy (middle panel), and the average scattering rate $\langle \nu_S^* \rangle$ for each simulation (bottom panel), as functions of the initial value of $\beta_{i\parallel}$. We note that the scattering rate ν_S^* at each time step was not calculated using Eq. 3. Instead, in order to make a more straightforward comparison with G+00, we used:

$$\nu_S^* \equiv -\frac{1}{A_i - 1} \left(\frac{\partial A_i}{\partial t} \right)_{scatt}, \quad (\text{A1})$$

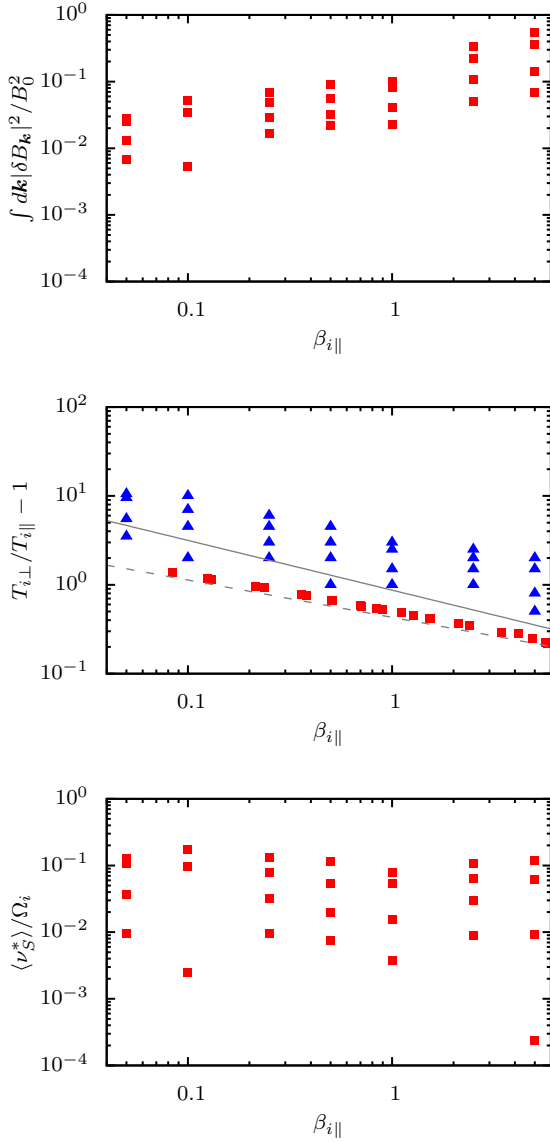


Figure A2. Results from the quasilinear calculations using a set of different initial conditions $(\beta_{i\parallel}, T_{i\perp}/T_{i\parallel})$ similar to those employed in the 2D hybrid simulations by Gary, Yin, & Winske (2000). Top panel: maximum magnetic energy density in the ion-cyclotron modes during the evolution. Middle panel: initial (blue triangles) and final (red squares) temperature anisotropy; the gray lines represent the thresholds (see Figure 1) for the ion-cyclotron (dashed) and mirror (continuous) instabilities. Bottom panel: average scattering rate of the ions normalized by the ion Larmor frequency.

and the time-average accounted only for values of $\nu_S^* \geq 0.6\nu_{\max}^*$, where ν_{\max}^* is the maximum instantaneous scattering rate during the time-evolution.

The results from Figure A2 are similar to those presented in Figure 2 in G+00, with differences no larger than one order of magnitude.

Figure A3 shows the relation between the average scattering rate $\langle \nu_S^* \rangle$ and the (initial) maximum growth rate of the unstable ion-cyclotron modes γ_{\max}^{IC} , for the same set of simulations. For comparison, it is also shown the (dashed

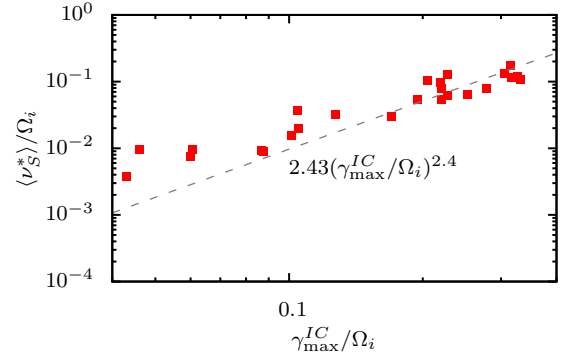


Figure A3. Average ions scattering rate $\langle \nu_S^* \rangle$ during the system evolution versus the maximum growth rate γ_{\max}^{IC} of the unstable ion-cyclotron modes. The dashed line represents the fitted curve in Gary, Yin, & Winske (2000).

line) fitting for this relation obtained by G+00. The quasilinear scattering rates agree at least in order of magnitude with the totally non-linear calculation, and the similarity is closer for the highest initial values of the ion-cyclotron growth rate.

This paper has been typeset from a $\text{\TeX}/\text{\LaTeX}$ file prepared by the author.